ACS OMEGA

Open Access

http://pubs.acs.org/journal/acsodf

Article

Nitrogen-Doped Carbon Dots: A New Powerful Fluorescent Dye with Substantial Effect on Bacterial Cell Labeling

Sin-Jen Lee, Ya-Yun Zheng, Wen-Ming Chen, and Yi-Huang Hsueh*

Cite This: *ACS Omega* 2024, 9, 36453−36463

Read Online

ACCESS | Metrics & More | Article Recommendations

ABSTRACT: Carbon dots (CDs)—minute carbon nanoparticles with remarkable luminescent properties, photostability, and low toxicity—show potential for various applications. CDs synthesized using citric acid and urea are the least toxic to biological environments. Here, we aimed to explore the effect of CDs synthesized using citric acid and urea at 50, 33, and 25% (CDs 1/1, 1/2, and 1/3, respectively) weight ratios in a microwave on bacterial cell fluorescence sensing and labeling. The nanoscale properties of CDs were investigated via transmission electron microscopy and dynamic light scattering particle size analysis. X-ray powder diffraction confirmed the graphitic structures of CDs. X-ray photoelectron spectroscopy revealed that the nitrogen content increased gradually with increasing urea ratios, indicating functional group changes. Transient photoluminescence decay periods demonstrated superior fluorescence intensity of CDs 1/3 under blue, green, and red lights. The use of CDs was notably more efficient than traditional methods in staining bacterial cells. Fluorescence microscopy of 10 g-positive and 10 g-negative bacteria revealed enhanced staining of Gram-positive strains, with CDs 1/3 presenting the best results. The CDs exhibited excellent photostability, maintaining poststaining fluorescence for 100 min, surpassing the performance of conventional dyes. CDs could serve as potential fluorescent dyes for the rapid discrimination of Gram-positive and Gram-negative bacteria.

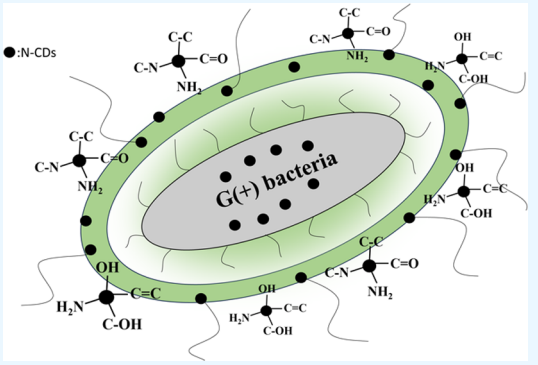

INTRODUCTION

The fluorescence mechanisms of carbon dots (CDs) and their interaction with bacteria are intricate and multifaceted. CDs emit a broad spectrum of light ranging from blue to red, influenced by variables such as carbon and nitrogen sources, synthesis conditions, and the carbon-to-nitrogen ratio.[1−3] Notably, the urea-to-citric acid ratio has emerged as a pivotal factor, affecting fluorescence emission with increased nitrogen content correlating to a shift toward deeper red fluorescence.[4−6] The fluorescence has been attributed to the radiative recombination of electrons transferring to surface functional groups upon excitation. In the context of bacterial binding, the interaction is mediated through surface defects or functional groups, thereby contributing to fluorescence emission upon binding.[7−9] The properties of CDs, including size, morphology, and surface chemistry, are amenable to precise control by manipulating critical reaction parameters such as precursor ratios, solvents, and reaction temperature.[10−13] This level of control holds significance in tailoring CDs to specific applications, ensuring their efficacy and safety. Citric acid and urea, ubiquitous components in food and pharmaceuticals, stand out as benign precursors for CD synthesis, ensuring lower cytotoxicity and enhanced environmental safety.[14] The synthesis process involving these precursors yields smaller and more stable CDs, minimizing potential adverse effects within biological systems. Extensive studies have underscored the efficacy of citric acid and urea as precursors, with ongoing investigations delving into the nuanced underlying mechanisms.[15] Though CDs can stain both Gram-positive and Gram-negative bacteria, they usually do not exclusively target Gram-positive bacteria.[16−18] Further, CDs can stain both live and dead bacteria, aiding in their differentiation.[19] CDs prepared using mannose and ammonium citrate as precursors demonstrate high specificity for *Escherichia coli*, as mannose serves as a target ligand covalently bound to the CD surface.[20] CDs modified with vancomycin substantially inhibit Gram-positive bacterial growth, because of the receptor−ligand interactions between the bacterial cell wall and vancomycin.[21] Furthermore, CDs synthesized using ammonia citrate effectively stain Gram-negative bacteria, showing specificity for *Helicobacter pylori*.[22] CDs@BONs have been prepared and used as fluorescent probes for the ultrasensitive detection of

Received: May 5, 2024
Revised: July 11, 2024
Accepted: August 8, 2024
Published: August 15, 2024

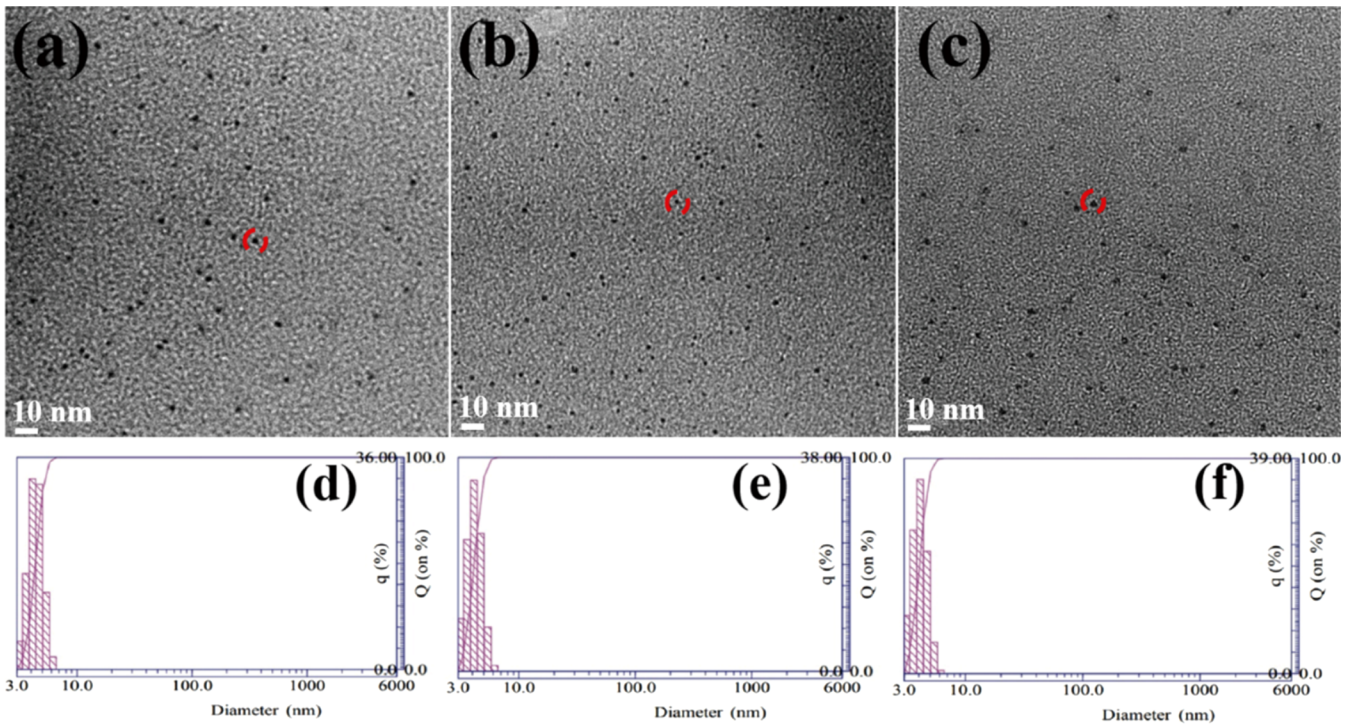

Figure 1. Particle size analysis of carbon dots (CDs). Analytical transmission electron microscopy micrographs of CDs. The (a) CD 1/1, (b) CD 1/2, and (c) CD 1/3 particles are shown at a low magnification (100,000×). The average particle sizes are as follows: (d) CDs 1/1, 4.3 nm; (e) CDs 1/2, 4.1 nm; and (f) CDs 1/3, 4.1 nm.

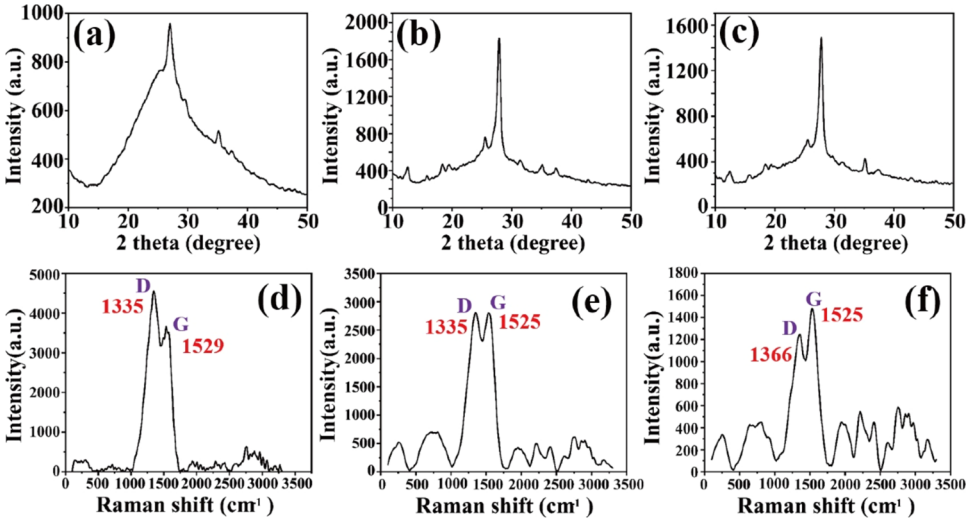

Figure 2. X-ray powder diffractometer analysis of the microstructure of carbon dots (CDs). (a) CDs 1/1 have a diffraction peak at 27.1°, (b) CDs 1/2 have a diffraction peak at 27.9°, and (c) CDs 1/3 have a diffraction peak at 27.8°. Raman spectra of CDs with different carbon-to-nitrogen ratios: (d) CDs 1/1, (e) CDs 1/2, and (f) CDs 1/3.

Staphylococcus aureus. Anti-*S. aureus* antibody-modified CDs@BONs have been used for specific labeling, with the CDs released from BONs via $NaBH_4$ reduction prior to fluorescence detection, achieving a linear range of 1−200 cfu/mL.[23] Traditional bacterial differentiation methods, notably Gram staining, necessitate alternatives because of inherent limitations. Enzyme-based assays, polymerase chain reaction-based techniques, and chemical treatments have emerged as promising avenues for swift and reliable bacterial identification.[24−28] These advancements not only pave the way for real-time monitoring but also offer avenues for the comprehensive assessment of bacterial viability. The interaction between CDs and bacteria involves a myriad of forces, encompassing electrostatic and nonspecific binding to proteins. The ζ-potential, indicative of bacterial negative charge, crucially influences nanoparticle adsorption, elucidating a straightforward adsorption mechanism in the bacteria−nanoparticle system.[29] Additionally, functional groups quantified using X-ray photoelectron spectroscopy (XPS) engage in hydrogen bonding with proteins, augmenting effective cell staining.[30] In summary, using citric acid and urea as precursors for CD synthesis is a safe and an effective strategy, characterized by low cytotoxicity and high biocompatibility. The fluorescence mechanisms and bacterial interactions are

https://doi.org/10.1021/acsomega.4c04273
ACS Omega 2024, 9, 36453−36463

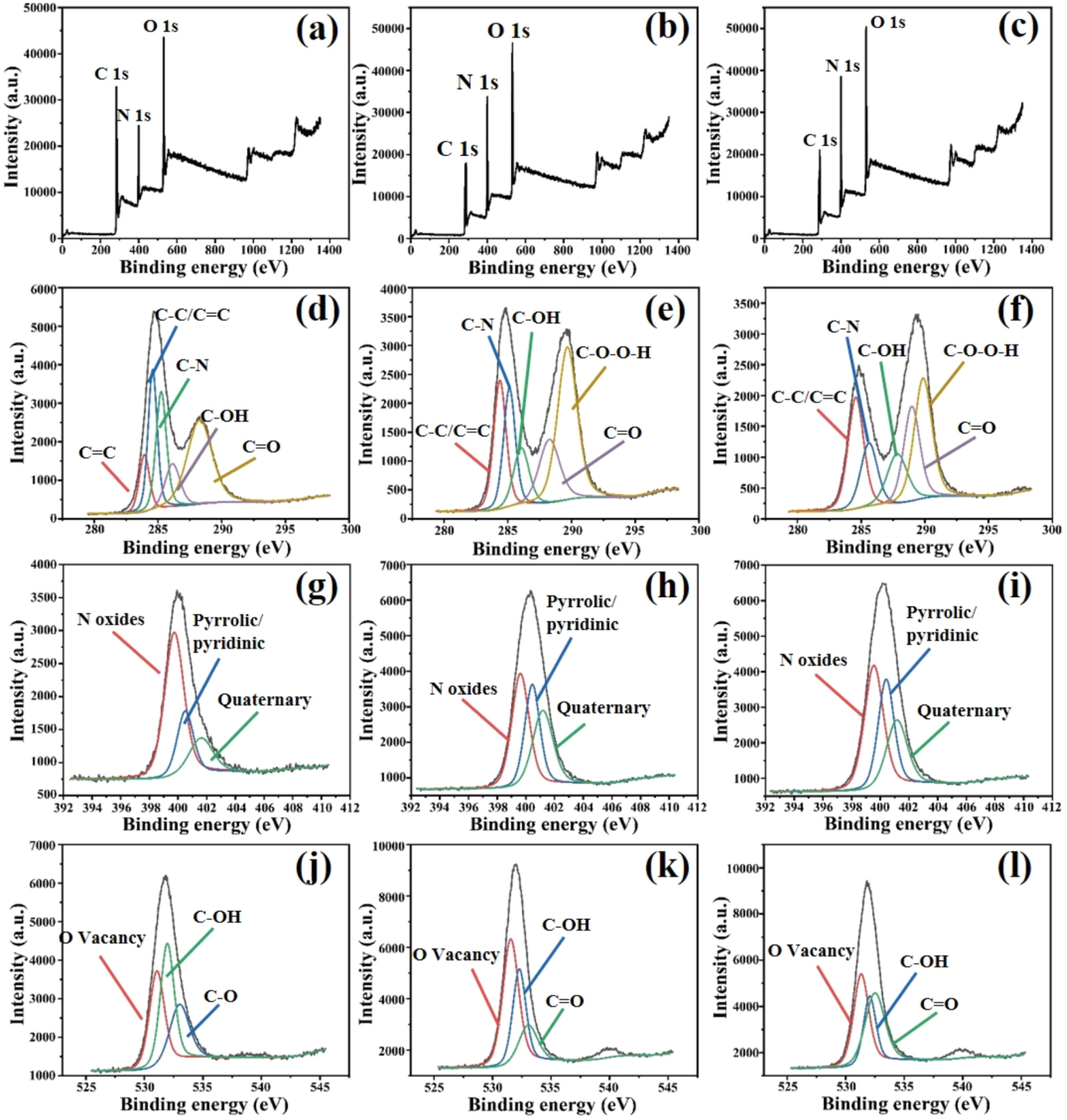

Figure 3. X-ray photoelectron spectra of carbon dot (CD) samples: (a–c) are the CD 1/1, 1/2, and 1/3 component peaks, respectively. (d–f) are the CDs 1/1 C 1s, N 1s, and O 1s peaks, respectively, deconvoluted by a multiple Gaussian function. (g–i) are the CD1/2 C 1s, N 1s, and O 1s peaks, respectively, deconvoluted by a multiple Gaussian function. (j–l) are the CD1/3 C 1s, N 1s, and O 1s peaks, respectively, deconvoluted by a multiple Gaussian function.

complex, influenced by surface states, functional groups, and experimental conditions. Ongoing research on alternative bacterial identification methods, along with real-time monitoring ability of CDs in bacterial staining and sensing, highlights a dynamic field that requires further exploration. To the best of our knowledge, this is the first study to demonstrate the use of CDs for Gram staining. We found that increasing nitrogen content significantly influences the fluorescence properties of CDs and the characteristics of fluorescent dyes. Bacterial staining experiments revealed that CDs can act as a novel fluorescent dye for rapid staining, and this approach could be an alternative to the traditional Gram staining.

RESULTS AND DISCUSSION

To determine the structural characteristics of CDs with different carbon-to-nitrogen ratios (CDs 1/1, 1/2, and 1/3), we conducted characterization studies using transmission electron microscopy (TEM), dynamic light scattering (DLS),

https://doi.org/10.1021/acsomega.4c04273
ACS Omega 2024, 9, 36453–36463

X-ray diffraction, Raman spectroscopy, and XPS. The morphology and microstructure of the CDs (CDs 1/1, 1/2, and 1/3) were observed using TEM. The self-synthesized CDs 1/1, 1/2, and 1/3 exhibited a spherical morphology and aggregation phenomenon (Figure 1a−c). ImageJ was used to measure the size of CDs 1/1, 1/2, and 1/3, and their average sizes were 3.1, 4.1, and 5.2 nm, respectively (all were smaller than 10 nm). The average size of the CDs in this study was determined using DLS. The average size of CDs 1/1 was 4.3 nm (Figure 1d) and that of CDs 1/2 was 4.1 nm (Figure 1e). The average size of CDs 1/3 was 4.1 nm (Figure 1f). The findings indicate that all three types of nano CDs (CDs 1/1, 1/2, and 1/3) were in the nanometer size range of 1−100 nm.

Generally, the (002) crystal plane diffraction peak of the graphite carbon structure is located at around 27°. In Figure 2a, the diffraction peak of CDs 1/1 is at 27.1°, whereas in Figure 2b, the diffraction peak of CDs 1/2 is at 27.9°. In Figure 2c, the diffraction peak of CDs 1/3 is at 27.8°. The diffraction peaks of the three CDs with different carbon-to-nitrogen ratios were within the range of the (002) crystal plane diffraction peak of the carbon structure, indicating their graphite structure. The diffraction peaks of the three CDs with different nitrogen ratios in Figure 2a−c were within the range of the (002) crystal plane diffraction peak of carbon, preliminarily proving their graphite structure. Figure 2d shows that the characteristic peak at 1,335 cm^{-1} in CDs 1/1 is attributable to the D band and that the peak at 1529 cm^{-1} is attributable to the G band, with an I_D/I_G intensity ratio of 1.24. Figure 2e shows that the characteristic peak at 1335 cm^{-1} in CDs 1/2 is attributable to the D band and that the peak at 1525 cm^{-1} is attributable to the G band, with an I_D/I_G intensity ratio of 1.0. Figure 2f shows that the characteristic peak at 1366 cm^{-1} in CDs 1/3 is attributable to the D band and that the peak at 1525 cm^{-1} is attributable to the G band, with an I_D/I_G intensity ratio of 0.84. The D band reflects lattice defects, and the use of an improved stone milling structure reduces its characteristic peak. The G band and I_D/I_G ratio reflect the number or thickness of graphite layers and density of defects in CDs, respectively. Generally, an I_D/I_G ratio of <1.0 indicates the presence of a crystalline component in CDs and that of <0.5 indicates a superior structure for CDs.[31] The I_D/I_G value for a graphite structure is around 1 ± 0.1. Based on the results shown in Figure 2, the I_D/I_G intensity ratio of CDs 1/2 was within this value, indicating a relatively good graphite structure.

Figure 3 shows the XPS analysis results of all three CDs, revealing the functional groups present. Figure 3a−c shows the C, N, and O content in the CDs 1/1, 1/2, and 1/3 nanocomposites, respectively, where a higher intensity represents a higher content of that element in all CDs. Figure 3d shows the peaks of C−C/C═C and C−N at 284.58 and 285.25 eV, respectively, whereas the peaks of C═C, C═O, and C−OH are at 283.93, 288.26, and 286.14 eV, respectively. In Figure 3g, the characteristic peaks at 399.74, 400.50, and 401.61 eV indicate the presence of N oxides, pyrrolic/pyridinic groups, and quaternary groups, respectively.[32] In addition, the high-intensity peaks at approximately 531.07, 533.01, and 531.96 eV represent O vacancies, C−OH, and C−O, respectively (Figure 3j). Figure 3e shows that the peaks for C−C/C═C and C−N are at 284.38 and 285.13 eV, respectively, whereas the peaks for C−OH, C═O, and C−O−O−H are at 286.06, 288.26, and 289.67 eV, respectively. In Figure 3h, the characteristic peaks at 399.62, 400.45, and 401.18 eV indicate the presence of N oxides, pyrrolic/pyridinic groups, and quaternary groups, respectively. Additionally, the high-intensity peaks at approximately 531.54, 532.28, and 533.04 eV represent O vacancies, C−OH, and C═O, respectively (Figure 3k). Figure 3f shows that the peaks for C−C/C═C and C−N are at 284.58 and 285.62 eV, respectively, whereas the peaks for C−OH, C═O, and C−O−O−H are at 287.83, 288.97, and 289.86 eV, respectively. In Figure 3i, the characteristic peaks at 399.55, 400.41, and 401.16 eV indicate the presence of N oxides and pyrrolic/pyridinic and quaternary functional groups, respectively. In addition, the high-intensity peaks at approximately 531.32, 532.05, and 532.49 eV represent O vacancy, C−OH, and C═O, respectively (Figure 3l).

CDs are primarily composed of citric acid and urea, and they possess distinctive chemical bonds such as C−N, pyrrolic/pyridinic N, C═C/C−C, and C−OH or C═O.[33,34] The surfaces of CDs are abundant in −OH and $-NH_2$ groups.[35] Although CDs exhibit similar levels of oxidation, the degree of amide formation varies.[36] The presence of pyrrolic/pyridinic N suggests nitrogen−carbon bonding in the five-membered ring systems of the synthetic material. Nitrogen-doped CDs are likely to be sp^2 aromatic and aromatic C−N, with abundant nitrogen-containing functional groups that originate from the urea component during the microwave synthesis process.[37] With the increase in the level of urea, the intensity of the N 1s peak also increased (Figure 3a−c). This increase may be because urea is a source of nitrogen. As the proportion of urea increased, the measured nitrogen content also increased, resulting in an increase in the intensity of N 1s.

The results of XPS analysis are listed in Table 1. The results of elemental analysis in CDs using an elemental analyzer revealed that the nitrogen content increased gradually with the addition of urea (Table 2), which was consistent with the results of the XPS analysis.

Table 1. X-ray Photoelectron Spectroscopy Analysis Showing Different Percentages of Bound Groups in the 1/1, 1/2, and 1/3 Carbon Dot Samples[a]

synthesized sample	element ratio (mol %)		
	CDs 1/1	CDs 1/2	CDs 1/3
	C 1s peak		
total	100	100	100
C−C or C═C	22.99	22.52	19.40
C−N	26.66	26.00	22.78
C−OH	29.56	29.07	29.41
C═O	20.79	22.41	28.41
	N 1s peak		
total	100	100	100
pyrrolic/pyridinic N	31.77	45.12	46.40
quaternary N	18.57	21.72	16.94
N oxides	49.66	33.16	36.66
	O 1s peak		
total	100	100	100
O vacancy	29.51	31.88	32.21
C−OH	45.37	50.46	43.08
C═O	25.12	17.66	24.71

[a]CD, carbon dot; C, carbon; H, hydrogen; O, oxygen; and N, nitrogen.

Figure 4a shows the absorption peaks of CDs 1/1 at 338 and 410 nm, which may be attributed to the $\pi-\pi$ transition of C═O. Figure 4b shows the absorption peaks of CDs 1/2 at 330

https://doi.org/10.1021/acsomega.4c04273
ACS Omega 2024, 9, 36453−36463

Table 2. Total Content of Nitrogen, Carbon, Hydrogen, and Oxygen in Carbon Dots 1/1, 1/2, and 1/3, as Analyzed Using an Elemental Analyzer[a]

sample	N%	C%	H%	O%
CDs 1/1	22.13	39.14	4.716	37.96
CDs 1/2	28.28	33.928	4.223	34.5
CDs 1/3	30.52	32.187	4.148	33.44

[a]CD, carbon dot; C, carbon; H, hydrogen; O, oxygen; and N, nitrogen.

and 412 nm, which may also be attributed to the $\pi-\pi$ transition of C═O. Figure 4c shows the absorption peaks of CDs 1/3 at 333 and 412 nm, which may also be attributed to the n-π transition of C═O. Generally, absorption spectra have only one maximum peak. However, two peaks can be clearly observed in Figure 4a−c. This might be because of the aggregation of different nitrogen-doped CDs (CDs 1/1, 1/2, and 1/3), as observed in the TEM image in Figure 1. The aggregation of the CDs formed a larger composite of CDs. Therefore, when the instrument was used for analysis and the light beam was irradiated onto the nanocarbon composite formed by aggregation, two refraction peaks were observed.

As the excitation wavelength increased, the CDs exhibited excitation-dependent emission. In Figure 4d−f, the emission of the nanomaterials shifts toward the red end as the excitation wavelength increases from 300 to 500 nm, indicating a red-shift phenomenon, possibly because of the presence of C−N bonds and cyanuric acid. Upon comparing the fluorescence intensities of the four different nitrogen-doped CDs, we found that the intensity of blue fluorescence was the highest for CDs 1/2, followed by CDs 1/3 and CDs 1/1; the intensity of green fluorescence was the highest for CDs 1/3, followed by CDs 1/2 and CDs 1/1; and the intensity of red fluorescence was the highest for CDs 1/2, followed by CDs 1/3 and CDs 1/1. Upon combining the fluorescence intensities of the four different nitrogen-doped CDs, we found that the best CDs for blue, green, and red lights were CDs 1/3 and CDs 1/2, indicating that the nitrogen ratio affects the fluorescence effects and characteristics. The individual quantum yield value was 13.45, 19.42, and 22.26% for CDs 1/1, 1/2, and 1/3, respectively. The yield of CDs can increase with the nitrogen content;[38] hence, increasing urea content results in the corresponding increase of nitrogen content, thereby increasing the CD yield.[39]

In Figure 5, it is evident that CDs 1/1, 1/2, and 1/3 do not have the ability to stain Gram-negative bacteria, such as *E. coli*. This observation was consistent for six different Gram-negative bacterial strains, implying a general ineffectiveness of CDs 1/1, 1/2, and 1/3 in staining this bacterial type. Consequently, we shifted our focus toward Gram-positive bacteria. Figures 6 and 7 illustrate that, under identical exposure times and a CD concentration of 500 ppm, CDs 1/1, 1/2, and 1/3 manifest discernible fluorescence in blue, green, and red lights for both *Bacillus subtilis* NCIB 3610 and *Lactobacillus plantarum*. Notably, in a comparison of pixel values of CDs 1/1, 1/2, and 1/3 under red, green, and blue lights, CDs 1/3 exhibited a significantly higher pixel value. This increased pixel value indicates a brighter fluorescence of CDs 1/3, as corroborated by the fluorescence intensity results depicted in Figure 8 and detailed in Table 3. Moreover, this trend persisted for an additional set of six Gram-positive bacterial strains, all of which exhibited successful staining. The collective findings affirm that although CDs 1/1, 1/2, and 1/3 lack staining efficacy for Gram-negative bacteria, they demonstrate pronounced fluorescence and efficacy in staining Gram-positive bacterial strains; particularly, CDs 1/3 exhibit superior brightness compared to CDs 1/1 and CDs 1/2.

Figure 8 shows *L. plantarum* (a Gram-positive bacterium)-staining stability of the different nitrogen-doped CDs (CDs 1/1, 1/2, and 1/3). Fluorescence stability was measured at 0, 10, 30, and 100 min after staining, and no fluorescence weakening or quenching was observed. This finding indicates that the nitrogen-doped CDs synthesized in this study has good photostability. This finding may be attributed to electrostatic interactions.[40,41] In Gram-positive bacteria, peptidoglycan is the outermost layer, carrying both positive and negative charges.[42−44] CDs also possess both positive and negative charges, allowing them to interact with peptidoglycan and facilitating Gram-positive staining.[45] Upon entering the cell membrane, the aromatic structures in CDs (comprising five- or six-membered carbon rings) bind with the hydrophobic part of peptidoglycan, and their hydrophilic ends engage in hydrogen bonding, thereby inducing fluorescence.[46] In contrast, the outer layer of Gram-negative bacteria is composed of lipopolysaccharides with strong negative charges, which

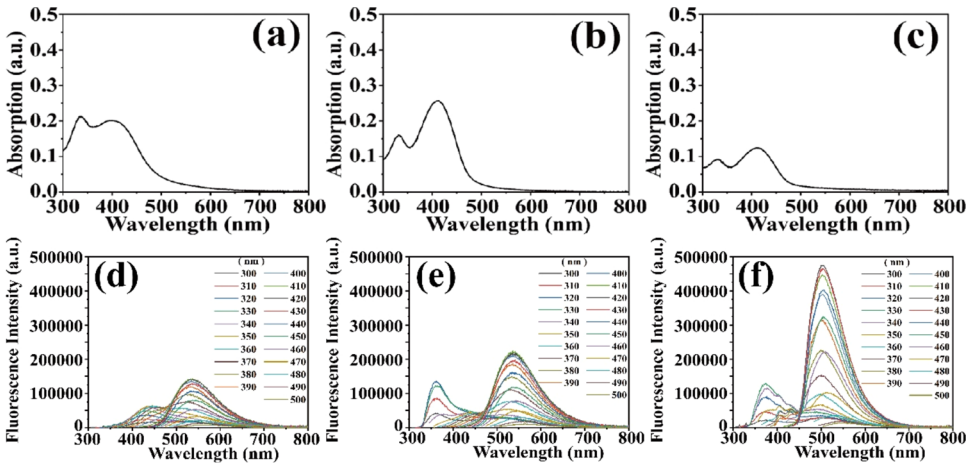

Figure 4. Ultraviolet−visible absorption spectra of carbon dots (CDs): (a) CDs 1/1, (b) CDs 1/2, and (c) CDs 1/3. Emission spectra obtained at excitation wavelengths of 300−500 nm for CDs: (d) CDs 1/1, (e) CDs 1/2, and (f) CDs 1/3.

https://doi.org/10.1021/acsomega.4c04273
ACS Omega 2024, 9, 36453−36463

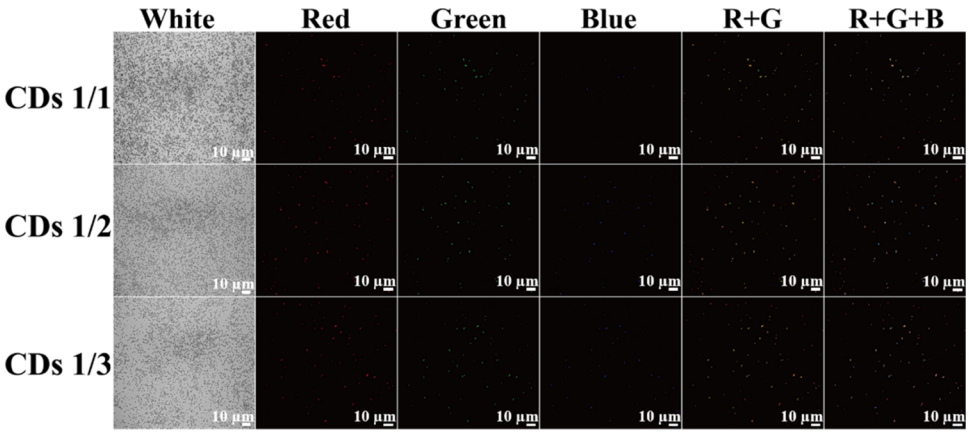

Figure 5. *E. coli* K12 fluorescence images of CDs with different carbon-to-nitrogen ratios (CDs 1/1, 1/2, and 1/3) at a concentration of 500 ppm. White dots are bacteria not stained with CDs 1/1, 1/2, or 1/3. The scale bar represents 10 μm. R, red; G, green; B, blue; and CD, carbon dot.

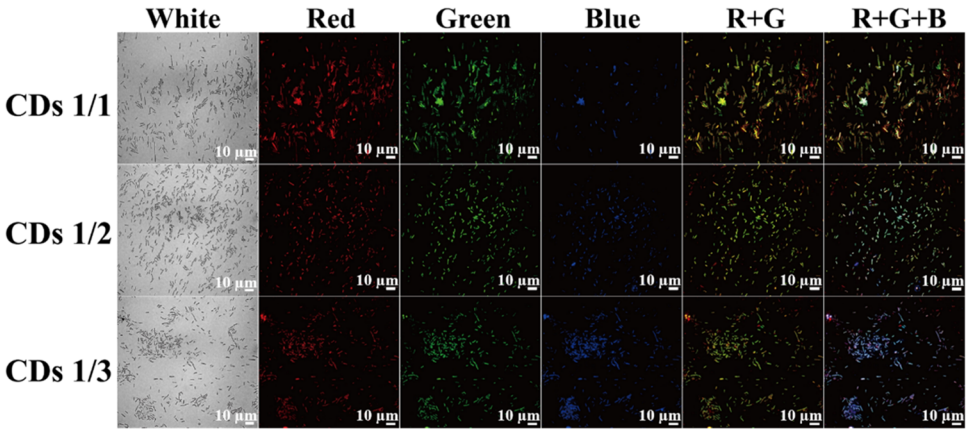

Figure 6. *B. subtilis* NCIB 3610 fluorescence images of CDs with different carbon-to-nitrogen ratios (CDs 1/1, 1/2, and 1/3) at a concentration of 500 ppm. White dots are bacteria not stained with CDs 1/1, 1/2, or 1/3. The scale bar represents 10 μm. R, red; G, green; B, blue; and CD, carbon dot.

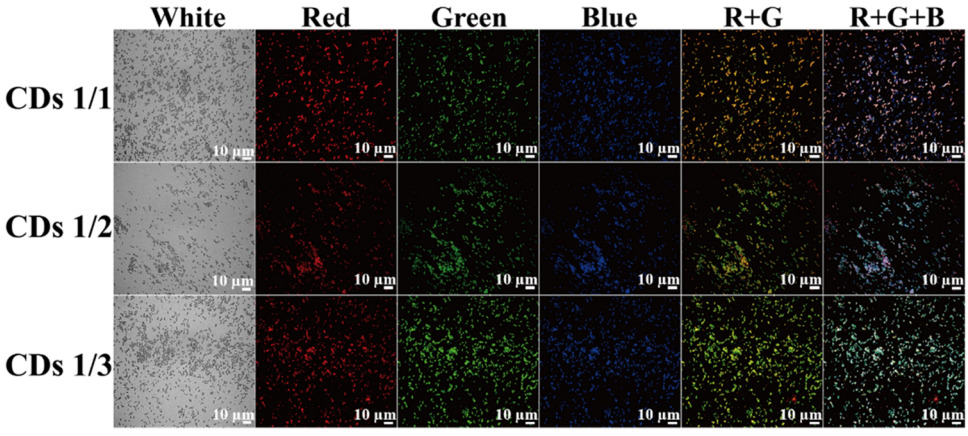

Figure 7. *L. plantarum* fluorescence images of CDs with different carbon-to-nitrogen ratios (CDs 1/1, 1/2, and 1/3) at a concentration of 500 ppm. White dots are bacteria not stained with CDs 1/1, 1/2, or 1/3. The scale bar represents 10 μm. R, red; G, green; B, blue; and CD, carbon dot.

possibly repel the negative charges on CDs.[47] Additionally, Gram-negative bacteria have an outer membrane composed of a lipid bilayer[48,49] that is resistant to hydrophobic interactions. The water solubility of CDs is hindered by the outer membrane, preventing the staining of Gram-negative bacteria. Furthermore, structural complexity is another factor contributing to differences in bacterial staining. Gram-positive bacteria are more easily stained by CDs than Gram-negative bacteria because of their simpler structures.[50]

Bacterial Staining Mechanism with CDs 1/1, 1/2, and 1/3. Figures 7 and 8 indicate the effective penetration of the dye into the bacterial cells for staining. However, it is not clear whether the staining is localized to the cell membrane or involves the entire bacterial cell. The scanning electron microscopy (SEM) image of *B. subtilis* NCIB 3610 without

https://doi.org/10.1021/acsomega.4c04273
ACS Omega 2024, 9, 36453−36463

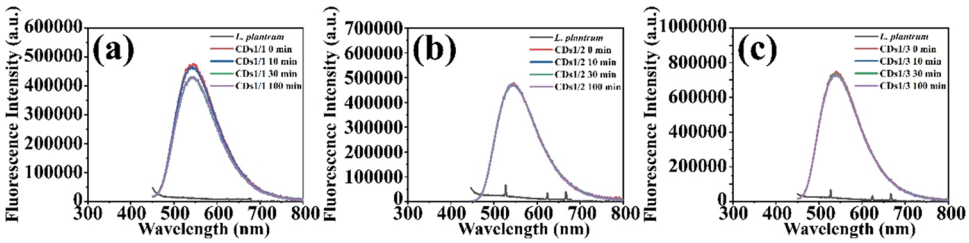

Figure 8. Determination of photostability of the Gram-positive bacteria *L. plantarum* with carbon dots of different nitrogen ratios. CD, carbon dot; *L. plantarum*, *Lactobacillus plantarum*.

Table 3. Analysis of Fluorescence Intensity of 1/1, 1/2, and 1/3 Carbon Dot Samples[a]

	B. subtilis NCIB 3610	*L. plantarum*
exposure time phase	70 ms	70 ms
exposure time red	4000 ms	4000 ms
exposure time green	2000 ms	3500 ms
exposure time blue	930 ms	1400 ms
	CDs 1/1	
pixel value red	1127	1100
pixel value green	2256	3197
pixel value blue	1772	2874
	CDs 1/2	
pixel value red	1047	1022
pixel value green	2263	3233
pixel value blue	1877	2868
	CDs 1/3	
pixel value red	1148	1775
pixel value green	2678	3799
pixel value blue	1912	3121

[a]CD, carbon dot.

CDs 1/3 presented in Figure 9a shows a uniformly smooth bacterial cell surface. Similarly, the SEM image of cells with CDs 1/3 shows a surface comparable to that of the control group (Figure 9b). The TEM image of cells without CDs 1/3 shows pristine bacterial cells and membranes (Figure 9c). Conversely, the TEM image of cells with CDs 1/3 clearly shows that CDs 1/3 infiltrated both the bacterial membrane and cells (Figure 9d). The conclusive evidence shown in Figure 9 supports the notion that CDs effectively stain the entire bacterial cell. Furthermore, we examined eight other Gram-positive bacteria and eight Gram-negative bacteria. All Gram-positive bacteria, with both high GC and low GC content, were stained. However, not all Gram-negative bacteria were stained with these CDs. These findings indicate that the CDs selectively stain only Gram-positive bacteria.

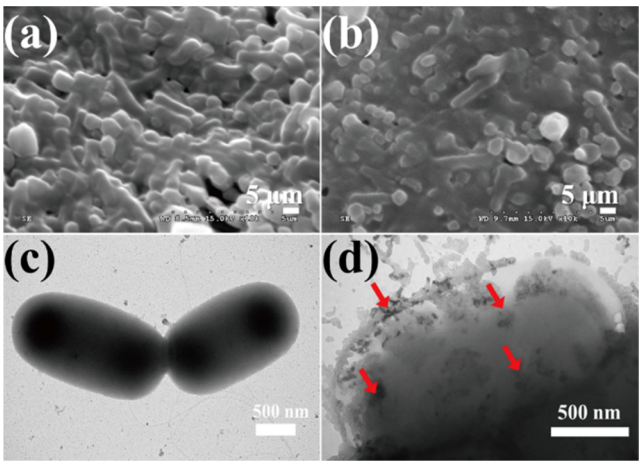

Figure 9. (a) Scanning electron microscopy (SEM) image of *B. subtilis* NCIB 3610 without added carbon dots (CDs) 1/3. (b) SEM image of *B. subtilis* NCIB 3610 with added CDs 1/3. (c) Transmission electron microscopy (TEM) image of *B. subtilis* NCIB 3610 without added CDs 1/3. (d) TEM image of *B. subtilis* NCIB 3610 with added CDs 1/3.

ζ-Potential Analysis of CDs 1/1, 1/2, and 1/3. The assessment of ζ-potential is crucial for evaluating the surface electrostatic properties of CDs in a dispersed system and plays a major role in the dispersion stability and interactions of carbon. We determined the ζ-potential of CDs 1/1, 1/2, and 1/3 with different carbon-to-nitrogen ratios at 1000 ppm, an electric field of −16.17 V/cm, and a mobility of −1.800e-004 $cm^2/(V{\cdot}s)$. The measurements were conducted using a DLS particle size analyzer and ζ-potential analyzer. CDs possess both positive and negative charges. The ζ-potential analyzer generated five potential values for the solution, which were then averaged to determine the final ζ-potential of the CDs. The ζ-potential values of the CDS were as follows: CDs 1/1 = −27.12 mV, CDs 1/2 = −28.29 mV, and CDs 1/3 = −34.09 mV. These values indicate the predominance of negative charges during CD measurements. A ζ-potential falling within the ±10 to ±30 range suggests slightly stable suspension particles (CDs), whereas that within the ±30 to ±40 range indicates moderately stable suspension particles (CDs). Larger values signify better solution stability and a reduced tendency for aggregation and precipitation (Beibei Wang et al., 2014). Therefore, it was concluded that the CDs 1/3 solution was comparatively more stable, as its ζ-potential lies within the optimal range.

Cell Toxicity Assessment of CDs 1/1, 1/2, and 1/3. The cytotoxicity of CDs was evaluated in 3T3-L1 normal cells, which are more sensitive than cancer cells. The toxicity of CDs 1/1, 1/2, and 1/3 against 3T3-L1 normal cells was measured using the cell counting kit-8 method. Compared with that in the control group, the growth of 3T3-L1 cells gradually decreased with increasing concentrations of CDs 1/1, 1/2, and 1/3 (10, 100, 200, and 500 ppm). Typically, a more than 3-fold decrease in values indicates significant toxicity. In our study, the decrease in cell growth was minimal, ranging from 0 to 0.1, with no significant differences (data not shown), indicating that the in-house generated CDs exhibited extremely low cytotoxicity. Therefore, CDs 1/1, 1/2, and 1/3 produced in this study are less likely to negatively affect the environment and living organisms.

https://doi.org/10.1021/acsomega.4c04273
ACS Omega 2024, 9, 36453−36463

CONCLUSIONS

CDs 1/1, 1/2, and 1/3 were confirmed as nanoscale materials using TEM and DLS analyses. The X-ray diffraction results indicate a graphene-like structure in CDs 1/1, 1/2, and 1/3. The Raman analysis highlighted the superior carbon crystallinity of CDs 1/3. The time-resolved photoluminescence (TRPL) findings showed that CDs 1/3 exhibited the strongest fluorescence across blue, green, and red lights with an impressive quantum yield of 22.26%. In the analysis of practical bacterial staining applications, all three CDs efficiently stained Gram-positive bacteria, with CDs 1/3 demonstrating the brightest fluorescence at the same exposure time. SEM and TEM provided visual evidence of CD-penetrating bacterial cells, facilitating fluorescent staining. The toxicity evaluation in 3T3-L1 normal cells revealed negligible differences between the CD and control groups, indicating minimal cytotoxicity of CDs 1/1, 1/2, and 1/3. The ζ-potential analysis confirmed the superior stability of CDs 1/3, with reduced tendencies for aggregation or precipitation, compared with that of CDs 1/1 and 1/2. In summary, CDs 1/3 emerged as the best candidate among the CDs with three different carbon-to-nitrogen ratios, demonstrating superior characteristics. The experimental results emphasize the influence of carbon content on the fluorescence effects and characteristics of the CDs. The bacterial staining experiment underscores the potential of CDs as innovative fluorescent dyes for rapid staining, potentially supporting traditional Gram staining methods.

MATERIALS AND METHODS

Synthesis of CDs. Nano CD composite materials with different carbon-to-nitrogen ratios, namely CDs 1/1, 1/2, and 1/3, were prepared using microwave. Citric acid and urea were added to 500 mL beakers at ratios of 1:1, 1:2, and 1:3, respectively. Approximately 40 mL of distilled water was added to each beaker, and the mixtures were stirred with a magnetic stirrer until there were no visible particles. After confirming that the solution was uniformly mixed, the mixtures were placed in a microwave oven (800 W, 12 A) and microwaved for 30 min until carbonization was complete. The beakers were removed, and the black solid residue from the beakers was scraped into a mortar, ground to a fine powder with a pestle, and stored in tubes as 1/1, 1/2, and 1/3 nano CD composite materials in a cool environment. Subsequently, the supernatant of CDs was prepared. The ground CD 1/1, 1/2, and 1/3 nanomaterials were added to 100 mL of distilled water, shaken thoroughly with a shaker, and centrifuged (6000 rpm). The supernatant was then poured into a tube and stored. This process was repeated twice, and the supernatant was then passed through a 0.45-μL filter membrane to obtain the supernatants of CDs 1/1, 1/2, and 1/3. The obtained supernatant was freeze-dried to obtain the nanocomposite materials of CDs 1/1, 1/2, and 1/3 with different carbon to nitrogen ratios. Yield of CDs (%) = (mass of CDs produced/mass of starting material) × 100

Characterization of CDs. TEM (JEM 3010; JEOL, Tokyo, Japan) was used to analyze the shape, size, and distribution of CD particles at 200 kV. A DLS particle size analyzer (HORIBA, Japan) was used to determine the size of CDs at 20 kHz. XPS (Fison VG ESCA210; West Sussex, U.K.) equipped with a Mg−Kα radiation emitter was used to analyze the chemical composition of the sample. C 1s, N 1s, and O 1s spectra were deconvoluted using a symmetric nonlinear least-squares algorithm with Gaussian functions. Ultraviolet−visible spectroscopy (UV−vis; CARY60) was used to detect the wavelength of the maximum absorption peak. A TRPL spectrometer (Edinburgh Instrument/FS5, U.K.) was used to detect the emission fluorescence intensity of CDs 1/1, 1/2, and 1/3 after absorption at excitation wavelengths of 300−500 nm. All experimental data represent the results of three independent experiments. An X-ray powder diffractometer (XRD; Bruker D2 Phaser, Germany) with an 18 kW rotating anode Cu target was used to analyze the microstructure of CDs. A three-dimensional (3D) nanometer-scale Raman photoluminescence (PL) microspectrometer system (Nanofinder 30, Tokyo, Japan) was used to study the vibrational modes of lattice molecules.

Fluorescence of CDs. A fluorescence microscope was used to observe the luminescence of different nitrogen-to-carbon ratio nanocomposites (CDs). The following bacteria were used: Gram-positive bacteria: *B. subtilis* NCIB 3610, *Bifidobacterium bifidum* ATCC 29521, *Bifidobacterium longum* ATCC 15708, *Lactobacillus rhamnosus* ATCC 21052, *L. plantarum* ATCC 14917, *Lactobacillus acidophilus* ATCC 4356, *Williamsia piscinae* CHRR-6, *Bacillus methylotrophicus*, *Bacillus aryabhattai* CEO-66, and *S. aureus* Newman; and Gram-negative bacteria: *E. coli* K12, *Cavicella fluminis* HSP-28, *Tabrizicola oligotrophica* Kms-5, *Pseudomonas* spp., *Novosphingobium trapae* TKW-15, *Litoribrevibacter euphylliae* Eupa-2, *Endozoicomonas acroprae* Acr-14, and *Thalassotalea euphylliae* Eup-16.

Luria−Bertani (LB) agar was used for culturing *B. subtilis* NCIB 3610, *S. aureus* Newman, *E. coli* K12, and *Salmonella*; de Man, Rogosa, and Sharpe (MRS) agar for *B. bifidum*, *B. longum*, *L. rhamnosus*, *L. plantarum*, and *L. acidophilus*; Reasoner's 2A (R2A) agar for *W. piscinae* CHRR-6, *B. methylotrophicus*, *B. aryabhattai* CEO-66, *C. fluminis* HSP-28, *T. oligotrophica* Kms-5, *Pseudomonas*, and *N. trapae* TKW-15; and MA agar for *L. euphylliae* Eupa-2, *E. acroprae* Acr-14, and *T. euphylliae* Eup-16 overnight. Test tubes were prepared and 5 mL of LB, MRS, R2A, and MA media was added. An inoculation loop to was used transfer the bacteria from agar plates to the test tubes, which were then incubated overnight at 37 °C and stored in a shaking incubator at 200 rpm. One milliliter of the cultured bacteria was centrifuged in an Eppendorf tube at 10,000 rpm for 3 min. The supernatant was discarded, and the pellet was washed with 1 mL of PBS, suspended, and centrifuged again at 10,000 rpm for 3 min. The supernatant was discarded and the pellet was used.

Preparation and Analysis of the TEM Chip. Carbon-coated copper grid chips (Support Films, Formvar/Carbon 400 mesh, Cu, Prod No. 01754-F; Ted Pella, Inc.) were prepared. Three different nitrogen-to-carbon ratio nanocomposites (CDs 1/1, 1/2, and 1/3) were prepared at a concentration of 500 ppm in a clearing solution. A pair of forceps was used to extract and fix the chip with a wooden clamp. Four microliters of each prepared nanocomposite solution was pipetted onto the carbon-coated copper grid chip and allowed to dry at room temperature (surface drying). After drying, the chip was placed in an empty Petri dish and incubated in a 25 °C oven for 2 d to completely evaporate the solution inside the chip. Finally, the chip was placed in the carbon-coated copper grid box. TEM (JEM 3010; JEOL, Tokyo, Japan) was used to determine the shape, size, and distribution of carbon particles in CDs at 200 kV.

https://doi.org/10.1021/acsomega.4c04273
ACS Omega 2024, 9, 36453−36463

DLS Particle Size Analysis. The DLS particle size analyzer used here had a particle size measurement range of 0.01−5,000 μm and a highest accuracy of ±0.6%, which is ideal for application to high concentration samples with a ppm of approximately 40 wt %. The supernatants of the three different nitrogen-to-CD nanocomposites (CDs 1/1, 1/2, and 1/3) were separately prepared at 100 ppm, and 20 mL of the samples was passed through a 0.45-μm filter in new tubes. The solution was placed in the DLS particle size analyzer, and the laser light generated scattered light upon impact with the particles. Particle size distribution was evaluated by measuring the variations in scattered light over time caused by the Brownian motion of particles.

X-ray Powder Diffraction Analysis. Each of the three different nitrogen-doped CD nanocomposites (CDs 1/1, 1/2, and 1/3) was used at 0.5−1.0 g in the powder form to determine the crystalline materials that are relatively abundant in the sample using an XRD. The 2θ scanning range was 10°−50°. The obtained diffraction data were compared with the International Centre for Diffraction Data to obtain the crystal structure.

3D Nanometer-Scale Raman PL Microspectrometer Analysis. Each of the three different nitrogen-doped CD nanocomposites (CDs 1/1, 1/2, and 1/3) at 0.05 g in the powder form was measured using a 3D Nanometer-Scale Raman PL Microspectrometer (Nanofinder 30). The Raman shift range was 0−3500 cm^{-1}, and the lattice vibration modes were observed. The specifications were as follows: HeNe laser, 632.8 nm; semiconductor laser, 488 nm; inverted microscope, Nikon Eclipse TE2000-U; XYZ scanning stage system, NT-MDT; XY resolution, 2 nm; Z resolution, 1 nm (in close-loop); and charge-coupled device detector, Andor DU401-BV.

UV−Vis Absorption Spectroscopy Analysis. The three different nitrogen-doped CDs (CDs 1/1, 1/2, and 1/3) were prepared as solutions at a concentration of 25 ppm, and 3 mL of the solutions was transferred into a glass cuvette. The samples were then subjected to UV−vis spectroscopy analysis using a UV−vis spectroscopy instrument with a UV−vis electromagnetic wave continuous spectrum as the light source. The relative intensity of light absorption by the molecules was studied, and qualitative analysis was performed to observe electronic transitions and absorption bands of the samples.

TRPL Spectrometry Analysis. The supernatants of the three different nitrogen-doped CD (CDs 1/1, 1/2, and 1/3) were prepared by diluting the samples to 25 ppm and transferring 3 mL of the supernatants into glass cuvettes. A TRPL spectrometer was used to detect their excitation and emission. This method is a powerful and nondestructive technique for detecting the optical properties of luminescent semiconductor materials. By analyzing the PL data, the type of doping impurities, band gap size, and impurity activation energy were determined from the spectral features.

AUTHOR INFORMATION

Corresponding Author

Yi-Huang Hsueh − *Department of Sea Food Science, National Kaohsiung University of Science, Kaohsiung 81157, Taiwan;* orcid.org/0000-0002-0838-7727; Email: yihhsueh@nkust.edu.tw

Authors

Sin-Jen Lee − *Department of Sea Food Science, National Kaohsiung University of Science, Kaohsiung 81157, Taiwan*

Ya-Yun Zheng − *Department of Sea Food Science, National Kaohsiung University of Science, Kaohsiung 81157, Taiwan*

Wen-Ming Chen − *Department of Sea Food Science, National Kaohsiung University of Science, Kaohsiung 81157, Taiwan*

Complete contact information is available at: https://pubs.acs.org/10.1021/acsomega.4c04273

Author Contributions

Conceived and designed the experiments: Y.H.H. Performed the experiments: S.J.L., Y.Y.Z. Analyzed the data: S.J.L., Y.Y.Z., W.M.C., Y.H.H. Contributed reagents/materials/analysis tools: Y.H.H., W.M.C. Wrote the paper: Y.H.H.

Notes

The authors declare no competing financial interest.

ACKNOWLEDGMENTS

We are grateful to Yan-Chen Chen from NKUST for her assistance with TEM data analysis and technical support. Her expertise and unwavering commitment were helpful in shaping the outcomes of this study. This research was funded by the National Science and Technology Council of Taiwan to Yi-Huang Hsueh, grant numbers 111-2221-E-992-023- and 112-2221-E992-012.

ABBREVIATIONS

CDcarbon dot; DLSdynamic light scattering; LBLuria−Bertani; PLphotoluminescence; TRPLtime-resolved photoluminescence; TEMtransmission electron microscopy; XPSX-ray photoelectron spectroscopy; XRDX-ray powder diffractometer

REFERENCES

(1) Miao, X.; Qu, D.; Yang, D.; Nie, B.; Zhao, Y.; Fan, H.; Sun, Z. Synthesis of carbon dots with multiple color emission by controlled graphitization and surface functionalization. *Adv. Mater.* **2018**, *30*, No. 1704740.

(2) Wang, B.; Lu, S. The light of carbon dots: From mechanism to applications. *Matter* **2022**, *5*, 110−149.

(3) Liu, H.; Zhong, X.; Pan, Q.; Zhang, Y.; Deng, W.; Zou, G.; Hou, H.; Ji, X. A review of carbon dots in synthesis strategy. *Coord. Chem. Rev.* **2024**, *498*, No. 215468.

(4) Vallan, L.; Imahori, H. Citric acid-based carbon dots and their application in energy conversion. *ACS Appl. Electron. Mater.* **2022**, *4*, 4231−4257.

(5) Sendão, R.; de Yuso, M. d. V. M.; Algarra, M.; da Silva, J. C. E.; da Silva, L. P. Comparative life cycle assessment of bottom-up synthesis routes for carbon dots derived from citric acid and urea. *J. Cleaner Prod.* **2020**, *254*, No. 120080.

(6) Kasprzyk, W.; Świergosz, T.; Romańczyk, P. P.; Feldmann, J.; Stolarczyk, J. K. The role of molecular fluorophores in the photoluminescence of carbon dots derived from citric acid: current state-of-the-art and future perspectives. *Nanoscale* **2022**, *14*, 14368−14384.

(7) Ding, H.; Yu, S. B.; Wei, J. S.; Xiong, H. M. Full-color light-emitting carbon dots with a surface-state-controlled luminescence mechanism. *ACS Nano* **2016**, *10*, 484−491.

(8) Ji, Z.; Yin, Z.; Jia, Z.; Wei, J. Carbon nanodots derived from urea and citric acid in living cells: Cellular uptake and antioxidation effect. *Langmuir* **2020**, *36*, 8632−8640.

(9) Park, Y.; Yoo, J.; Lim, B.; Kwon, W.; Rhee, S. W. Improving the functionality of carbon nanodots: doping and surface functionalization. *J. Mater. Chem. A* **2016**, *4*, 11582−11603.

(10) Anuar, N. K. K.; Tan, H. L.; Lim, Y. P.; So'aib, M. S.; Bakar, N. F. A. A review on multifunctional carbon-dots synthesized from

https://doi.org/10.1021/acsomega.4c04273
ACS Omega 2024, 9, 36453−36463

biomass waste: Design/fabrication, characterization and applications. *Front. Energy Res.* **2021**, *9*, No. 626549.
(11) Li, S.; Li, L.; Tu, H.; Zhang, H.; Silvester, D. S.; Banks, C. E.; Zou, G.; Hou, H.; Ji, X. The development of carbon dots: From the perspective of materials chemistry. *Mater. Today* **2021**, *51*, 188−207.
(12) Mansuriya, B. D.; Altintas, Z. Carbon dots: Classification, properties, synthesis, characterization, and applications in health care—An updated review (2018−2021). *Nanomaterials* **2021**, *11*, No. 2525.
(13) Wang, B.; Cai, H.; Waterhouse, G. I.; Qu, X.; Yang, B.; Lu, S. Carbon dots in bioimaging, biosensing and therapeutics: A comprehensive review. *Small Sci.* **2022**, *2*, No. 2200012.
(14) Qi, H.; Qiu, L.; Zhang, X.; Yi, T.; Jing, J.; Sami, R.; Alanazi, S. F.; Alqahtani, Z.; Aljabri, M. D.; Rahman, M. M. Novel N-doped carbon dots derived from citric acid and urea: Fluorescent sensing for determination of metronidazole and cytotoxicity studies. *RSC Adv.* **2023**, *13*, 2663−2671.
(15) Strauss, V.; Wang, H.; Delacroix, S.; Ledendecker, M.; Wessig, P. Carbon nanodots revised: The thermal citric acid/urea reaction. *Chem. Sci.* **2020**, *11*, 8256−8266.
(16) Das, P.; Ganguly, S.; Bose, M.; Mondal, S.; Choudhary, S.; Gangopadhyay, S.; Das, A. K.; Banerjee, S.; Das, N. C. Zinc and nitrogen ornamented bluish white luminescent carbon dots for engrossing bacteriostatic activity and Fenton based bio-sensor. *Mater. Sci. Eng., C* **2018**, *88*, 115−129.
(17) Choi, C. A.; Mazrad, Z. A. I.; Lee, G.; In, I.; Lee, K. D.; Park, S. Y. Boronate-based fluorescent carbon dot for rapid and selectively bacterial sensing by luminescence off/on system. *J. Pharm. Biomed. Anal.* **2018**, *159*, 1−10.
(18) Zheng, L.; Qi, P.; Zhang, D. Identification of bacteria by a fluorescence sensor array based on three kinds of receptors functionalized carbon dots. *Sens. Actuators, B* **2019**, *286*, 206−213.
(19) Song, Y.; Li, H.; Lu, F.; Wang, H.; Zhang, M.; Yang, J.; Huang, J.; Huang, H.; Liu, Y.; Kang, Z. Fluorescent carbon dots with highly negative charges as a sensitive probe for real-time monitoring of bacterial viability. *J. Mater. Chem. B* **2017**, *5*, 6008−6015.
(20) Lai, I. P.-J.; Harroun, S. G.; Chen, S.-Y.; Unnikrishnan, B.; Li, Y.-J.; Huang, C.-C. Solid-state synthesis of self-functional carbon quantum dots for detection of bacteria and tumor cells. *Sens. Actuators, B* **2016**, *228*, 465−470.
(21) Zhong, D.; Zhuo, Y.; Feng, Y.; Yang, X. Employing carbon dots modified with vancomycin for assaying gram-positive bacteria like Staphylococcus aureus. *Biosens. Bioelectron.* **2015**, *74*, 546−553.
(22) Geng, J.; Wang, Z.; Wu, Y.; Yu, L.; Yu, A.; Wang, L.; Dong, Q.; Liu, C.; Chi, Z. Intrinsic specificity of plain ammonium citrate carbon dots for Helicobacter pylori: Interfacial mechanism, diagnostic translation, and general revelation. *Mater. Today Bio* **2022**, *15*, No. 100282.
(23) Yang, L.; Deng, W.; Cheng, C.; Tan, Y.; Xie, Q.; Yao, S. Fluorescent immunoassay for the detection of pathogenic bacteria at the single-cell level using carbon dots-encapsulated breakable organosilica nanocapsule as labels. *ACS Appl. Mater. Interfaces* **2018**, *10*, 3441−3448.
(24) Alturkistani, H. A.; Tashkandi, F. M.; Mohammedsaleh, Z. M. Histological stains: A literature review and case study. *Global. J. Health Sci.* **2015**, *8*, No. 72.
(25) Ramírez-Guízar, S.; Sykes, H.; Perry, J. D.; Schwalbe, E. C.; Stanforth, S. P.; Perez-Perez, M. C. I.; Dean, J. R. A chromatographic approach to distinguish gram-positive from Gram-negative bacteria using exogenous volatile organic compound metabolites. *J. Chromatogr. A* **2017**, *1501*, 79−88.
(26) Vidic, J.; Vizzini, P.; Manzano, M.; Kavanaugh, D.; Ramarao, N.; Zivkovic, M.; Radonic, V.; Knezevic, N.; Giouroudi, I.; Gadjanski, I. Point-of-need DNA testing for detection of foodborne pathogenic bacteria. *Sensors* **2019**, *19*, No. 1100.
(27) Lan, H.; Shu, W.; Jiang, D.; Yu, L.; Xu, G. Cas-based bacterial detection: Recent advances and perspectives. *Analyst* **2024**, *149*, 1398−1415, DOI: 10.1039/D3AN02120C.
(28) Zhu, J.; Wang, B.; Zhang, Y.; Wei, T.; Gao, T. Living electrochemical biosensing: Engineered electroactive bacteria for biosensor development and the emerging trends. *Biosens. Bioelectron.* **2023**, *237*, No. 115480.
(29) Pajerski, W.; Ochonska, D.; Brzychczy-Wloch, M.; Indyka, P.; Jarosz, M.; Golda-Cepa, M.; Sojka, Z.; Kotara, A. Attachment efficiency of gold nanoparticles by gram-positive and gram-negative bacterial strains governed by surface charges. *J. Nanopart. Res.* **2019**, *21*, No. 186.
(30) Fu, C.-C.; Wu, C.-Y.; Chien, C.-C.; Hsu, T.-H.; Ou, S.-F.; Chen, S.-T.; Wu, C. H.; Hsieh, C. T.; Juang, R. S.; Hsueh, Y. H. Polyethylene Glycol6000/carbon nanodots as fluorescent bioimaging agents. *Nanomaterials* **2020**, *10*, No. 677.
(31) Dervishi, E.; Ji, Z.; Htoon, H.; Sykora, M.; Doorn, S. K. Raman spectroscopy of bottom-up synthesized graphene quantum dots: Size and structure dependence. *Nanoscale* **2019**, *11*, 16571−16581.
(32) Hsieh, C.-T.; Gu, S.; Gandomi, Y. A.; Fu, C.-C.; Sung, P.-Y.; Juang, R.-S.; Chen, C.-C. Employing functionalized graphene quantum dots to combat coronavirus and enterovirus. *J. Colloid Interface Sci.* **2023**, *630*, 1−10.
(33) Sordello, F.; Zeb, G.; Hu, K.; Calza, P.; Minero, C.; Szkopek, T.; Cerruti, M. Tuning TiO_2 nanoparticle morphology in graphene−TiO_2 hybrids by graphene surface modification. *Nanoscale* **2014**, *6*, 6710−6719.
(34) Wang, S.; Chen, H.; Xie, H.; Wei, L.; Xu, L.; Zhang, L.; Lan, W.; Zhou, C.; She, Y.; Fu, H. A novel thioctic acid-carbon dots fluorescence sensor for the detection of Hg^{2+} and thiophanate methyl via S-Hg affinity. *Food Chem.* **2021**, *346*, No. 128923.
(35) Mathew, S.; Thara, C. R.; John, N.; Mathew, B. Carbon dots from green sources as efficient sensor and as anticancer agent. *J. Photochem. Photobiol., A* **2023**, *434*, No. 114237.
(36) Gu, S.; Hsieh, C. T.; Yuan, C. Y.; Gandomi, Y. A.; Chang, J. K.; Fu, C. C.; Yang, J. W.; Juang, R. S. Fluorescence of functionalized graphene quantum dots prepared from infrared-assisted pyrolysis of citric acid and urea. *J. Lumin.* **2020**, *217*, No. 116774.
(37) Dwitya, S. S.; Hsueh, Y. H.; Wang, S. S. S.; Lin, K. S. Ultrafine nitrogen-doped graphene quantum dot structure and antibacterial activities against *Bacillus subtilis* 3610. *Mater. Chem. Phys.* **2023**, *295*, No. 127135.
(38) Uriarte, D.; Domini, C.; Garrido, M. New carbon dots based on glycerol and urea and its application in the determination of tetracycline in urine samples. *Talanta* **2019**, *201*, 143−148.
(39) Hao, R.; Xing, R.; Xu, Z.; Hou, Y.; Gao, S.; Sun, S. Synthesis, functionalization, and biomedical applications of multifunctional magnetic nanoparticles. *Adv. Mater.* **2010**, *22*, 2729−2742.
(40) Kung, J. C.; Tseng, I. T.; Chien, C. S.; Lin, S. H.; Wang, C. C.; Shih, C. J. Microwave assisted synthesis of negative-charge carbon dots with potential antibacterial activity against multi-drug resistant bacteria. *RSC Adv.* **2020**, *10*, 41202−41208.
(41) Thakur, M.; Dan, A. Poly-l-lysine-functionalized green-light-emitting carbon dots as a fluorescence turn-on sensor for ultra-sensitive detection of endotoxin. *ACS Appl. Bio Mater.* **2021**, *4*, 3410−3422.
(42) Reith, J.; Mayer, C. Peptidoglycan turnover and recycling in gram-positive bacteria. *Appl. Microbiol. Biotechnol.* **2011**, *92*, 1−11.
(43) Labischinski, H.; Maidhof, H.Bacterial Peptidoglycan: Overview and Evolving Concepts. In *New Comprehensive Biochemistry*; Elsevier, 1994; Chapter 2, Vol. *27*, pp 23−38.
(44) Vollmer, W.; Seligman, S. J. Architecture of peptidoglycan: More data and more models. *Trends Microbiol.* **2010**, *18*, 59−66.
(45) Yang, J.; Zhang, X.; Ma, Y. H.; Gao, G.; Chen, X.; Jia, H. R.; Li, Y. H.; Chen, Z.; Wu, F. G. Carbon dot-based platform for simultaneous bacterial distinguishment and antibacterial applications. *ACS Appl. Mater. Interfaces.* **2016**, *8*, 32170−32181.
(46) Devi, N.; Wangoo, N. Tuning the luminescence of microwave-assisted N-doped fluorescent carbon dots: Bioimaging applications and label-free anti-cancer drug delivery. *ACS Appl. Bio Mater.* **2023**, *6*, 999−1010.

https://doi.org/10.1021/acsomega.4c04273
ACS Omega 2024, 9, 36453−36463

(47) Lu, F.; Song, Y.; Huang, H.; Liu, Y.; Fu, Y.; Huang, J.; Li, H.; Qu, H.; Kang, Z. Fluorescent carbon dots with tunable negative charges for bio-imaging in bacterial viability assessment. *Carbon* **2017**, *120*, 95−102.
(48) Henderson, J. C.; Zimmerman, S. M.; Crofts, A. A.; Boll, J. M.; Kuhns, L. G.; Herrera, C. M.; Trent, M. S. The power of asymmetry: architecture and assembly of the gram-negative outer membrane lipid bilayer. *Annu. Rev. Microbiol.* **2016**, *70*, 255−278.
(49) Doerrler, W. T. Lipid trafficking to the outer membrane of gram-negative bacteria. *Mol. Microbiol.* **2006**, *60*, 542−552.
(50) Lin, F.; Bao, Y. W.; Wu, F. G. Carbon dots for sensing and killing microorganisms. *C-J. Carbon Res.* **2019**, *5*, No. 33.

https://doi.org/10.1021/acsomega.4c04273
ACS Omega 2024, 9, 36453−36463